Chapter 8
Corn Goss's Wilt Disease Assessment Based on UAV Imagery

Anup Kumar Das, Jithin Mathew, Zhao Zhang, Andrew Friskop, Yuxiang Huang, Paulo Flores, and Xiongzhe Han

Abstract Goss Wilt is a common and serious disease during corn production. With a goal of automatic disease monitoring, this study assessed Goss's Wilt disease severity using machine (ML) and deep learning (DL) algorithms. A dataset containing 200 corn plot images was generated from an unmanned aerial vehicle (UAV) flying at five

A. K. Das · J. Mathew · Z. Zhang (✉) · P. Flores
Department of Agricultural and Biosystems Engineering, North Dakota State University, Fargo, ND, USA
e-mail: zhao.zhang.1@ndsu.edu

A. K. Das
e-mail: anup.das@ndsu.edu

J. Mathew
e-mail: jithin.mathew@ndsu.edu

P. Flores
e-mail: paulo.flores@ndsu.edu

Z. Zhang
Key Lab of Modern Precision Agriculture System Integration Research, Ministry of Education of China, China Agricultural University, Beijing 100083, China

Key Lab of Agriculture Information Acquisition Technology, Ministry of Agriculture and Rural Affairs of China, China Agricultural University, Beijing 100083, China

A. Friskop
Department of Plant Pathology, North Dakota State University, Fargo, ND 58102, USA
e-mail: andrew.j.friskop@ndsu.edu

Y. Huang
College of Mechanical and Electronic Engineering, Northwest A & F University, Yangling, Shaanxi, China
e-mail: hyx@nwsuaf.edu.cn

X. Han
Department of Biosystems Engineering, College of Agriculture and Life Sciences, Kangwon National University, Chuncheon 24341, Korea
e-mail: hanxiongzhe@kangwon.ac.kr

Interdisciplinary Program in Smart Agriculture, College of Agriculture and Life Sciences, Kangwon National University, Chuncheon 24341, Korea

Z. Zhang et al. (eds.), *Unmanned Aerial Systems in Precision Agriculture*,
Smart Agriculture 2, https://doi.org/10.1007/978-981-19-2027-1_8

different mission heights (15, 30, 45, 60, and 75 m) above the ground level (AGL). Three different datasets including non-augmentation, segmentation and augmentation were prepared. The augmentation dataset consisting of 6200 images was prepared using geometric augmentation techniques, such as rotation, and flip. Eight different ML algorithms (i.e., Logistic Regression, Ada Boost, Gradient Boosting, Support Vector Machine, Multilayer Perceptron, Random Forest, Naive Bayes, K-Nearest Neighbors) and two different DL algorithms (i.e., GoogLeNet and ResNet18) were implanted to classify Goss Wilt severity as a binary issue (i.e., high and low). Two different types of features, including textural (contrast, dissimilarity, homogeneity, angular second moment) and color (hue, saturation, value, lightness, chromatic components: a* and b*, red, green, blue) features were extracted from individual plot image. For ML, the Random Forest yielded 0.99 precision, 0.99 recall and 0.99 F-score in augmented dataset and outperformed all other classifiers. For DL, Resnet18 achieved slightly better results: 0.81 precision, 0.78 recall and 0.79 F-score than GoogleNet, which has 0.75 precision, 0.70 recall, and 0.73 F-score. The ML model (Random Forest) performed satisfactorily by resulting in higher precision, recall and F-score in augmented dataset. However, ML models underperformed on segmentation dataset. Therefore, Random Forest coupled with UAV imagery is a potential valuable tool for automatic assessment of Goss Wilt disease.

Keywords Corn · Goss's Wilt · Machine learning · Deep learning

8.1 Introduction

Corn (*Zea mays L.*) accounts for more than 95% of the feed grain produced in the United States [27]. Goss's Wilt, a corn leaf disease, has been recognized as one of the most yield-limiting diseases, causing up to 50% production losses in North Dakota [5]. Field visits coupled with visual observation are used to assess Goss Wilt, which is time consuming (inefficiency), subjective, and leading to incorrect assessments due to evaluator's fatigue. As a result, developing an automated, quick, and reliable approach for Goss Wilt disease monitoring has been a top priority.

Unmanned aerial vehicles (UAVs) appear in a number of agricultural applications due to rapid and high-quality collected data, and ability to replace human labor for data collection [17]. The UAV imagery is now extensively used in agriculture for crop disease detection, such as citrus canker [1], vine disease [9, 10], yield monitoring for rice grain [12], glyphosate-resistant and glyphosate-susceptible weed and pest management [26], crop health monitoring of winter corn and barley [21]. Kerkech et al. [9] also used UAV imagery to develop automatic grape vine detection using a convolutional neural network (CNN) and achieved 96% detection accuracy.

Kerkech et al. [10] proposed UAV based automated vine disease detection system using deep learning (DL) techniques and achieved more than 92% detection accuracy. A majority of the existing studies focus on the identification of diseases. However, very few researchers extended the detection problem to the disease severity levels.

Liu et al. [14] developed a relationship between image parameters and wheat powdery mildew severity and achieved positive correlations. They extracted several features from the UAV images and found color features had a positive correlation with powdery mildew severity. Salgadoe et al. [23] used two different types of images (RGB and eight bands satellite image) for quantifying the severity of root rot disease of avocado and found promising results generated from the satellite images. However, limited study has been conducted using RGB color images for determining the severity of Goss's Wilt diseases.

Progress and applications of sensing and automation technology in agriculture have benefitted the agricultural production [7, 8, 15, 29, 30, 33–35]. The current advances in drone technology provide new ways in collecting crop information and assisting growers in decision making [3, 4, 31]. Researchers used machine learning (ML) techniques to detect corn leaf disease. Supervised ML pipeline involves data preparation, feature extractions, feature selection, training, testing, and validation. For ML algorithms, features (e.g., color, textural, and shape) are usually extracted manually, after which they are generally selected using selection algorithms and used for training. Ren et al. [22] extracted 129 features, including 30 color features, 9 shape features, and 90 textural features and observed shape features highly contributing to classify spot diseases in corn leaves. Panigrahi et al. [18] used ML techniques, including random forest (RF), decision tree (DT), and naive bayes (NB), to accurately identify corn leaf diseases. Support vector machine (SVM) classifier was used for corn leaf disease classification, which generated a high success rate of 87% by Meng et al. [16], 96% by Liu et al. [14] and 89% by Ren et al. [22]. Kusumo et al. [11] used SVM, DT, RF, and NB to distinguish healthy leaves from corn gray leaf spot, common rust, and leaf blight and achieved good performance from SVM with color features and RF with local features (Speeded Up Robust Features). Many studies utilized ML systems to predict the severity of plant leaf diseases [2, 13, 19, 24]. However, few studies on the severity of Goss Wilt disease in corn have been conducted.

In recent years, the use of DL in agriculture has grown considerably. Deep neural networks consisting of layers can learn high-level features from data. For feature extraction, ML needs domain knowledge, while DL can extract features automatically, and eliminate the need for human feature extraction and selection. Wang et al. [28] presented an automated plant disease severity assessment system based on VGG16, VGG19, Inception-v3, and ResNet50. They categorized apple leaf images into four groups: healthy, early, middle, and end stage of apple leaf black rot. They reported that the VGG16 model outperformed the VGG19, Inception-v3, and ResNet50 models, yielding a 90% accuracy. For categorizing and evaluating the severity of coffee leaf biotic into four categories (i.e., healthy, low, and very low), Esgario et al. utilized AlexNet, GoogLeNet, VGG16, ResNet50, and MobileNetV2 and effectively evaluated severity with 87% accuracy. DL methods, on the other hand, are data hungry and computationally expensive. With small dataset, training DL algorithms may easily result in model overfitting. Several studies trained DL algorithms using augmentation datasets to cope with small datasets and reduce the risk of model overfitting. Data augmentation is an artificial data enlargement technique that optimizes parameters and reduces model overfitting.

Researchers utilized data augmentation techniques including random rotation, shearing, zooming, and flipping, horizontal and vertical mirroring, rotation, and color brightness, contrast, and saturation (Esgario et al. 2020) [28] and observed uses of the techniques improved system accuracy. Zhang et al. [32] also observed 5% of accuracy improvement using data augmentation techniques. Thus, for small dataset, it is desirable to conduct data augmentation before training models.

With a final goal of realizing automatic corn Goss's Wilt disease detection, this study focuses on testing different ML and DL algorithms and then recommend the desirable one. Specific research objectives are to: (1) collect UAV images and then prepare the dataset, (2) train, test and compare different ML and DL algorithms, (3) Recommend a model for assessing Goss's Wilt disease.

8.2 Material and Methodology

8.2.1 Data Collection and Data Preprocessing

A field, located in Horace, North Dakota, U.S., was rented from a local farmer (Fig. 8.1). A DJI Phantom 4D RTK (DJI-Innovations, Inc., ShenZhen, China) drone equipped with a 20-megapixel 2.54 cm CMOS camera with 4864 × 3648 resolution and a high-precision (±10 cm) RTK GNSS system was utilized to capture image data on August 11, 2020, at 1:00 PM (local time; sunny). A total of five missions were carried out at five different flying heights, including 15, 30, 45, 60, and 75 m above ground level (AGL). The flights were set 80% of the side and front overlap and at a speed of 2.5 m/s. Following data collection, a plant pathologist visited each plot to manually and visually inspect the Goss's Wilt severity, which was categorized into two grades (high and low severity). The experimental plots (40 in total) were divided into two categories: high severity (23 in total) and low severity (17 in total).

The individual images obtained from the UAV for the five flight altitudes were automatically stitched using Pix4D software (Pix4D SA, Lausanne, Switzerland)

Fig. 8.1 Location of the field in Google Maps™ (Adapted from Google LLC., 2021)

and then cropped in ImageJ (ImageJ version 1.50e, USA; http://rsbweb.nih.gov/ij). Plots from the cropped images were generated using a plot splitting tool developed in this study (Fig. 8.2). A total of 200 plot images (40 plots/height × 5 heights) were generated. The developed tool took an image as input and divided it into a grid (4 × 10) for given input (column: 4 and row: 10) automatically where each cell represented a plot. The plot image dimensions (i.e., length and width) were calculated using Eqs. (8.1) and (8.2). A region of interest (ROI) was calculated by Eqs. (8.3) and (8.4) and placed in each cell using the function setRoi (xx, yy, roiw, roih) method. The function creates a rectangular selection on the image for cropping and saving plots.

$$ROI\ witdh = \frac{Image\ width}{Total\ number\ of\ column} \tag{8.1}$$

$$ROI\ height = \frac{Image\ height}{Total\ number\ of\ row} \tag{8.2}$$

$$ROI\ position\ (xx) = i * ROI\ witdh \quad where\ i < Total\ number\ of\ column \tag{8.3}$$

$$ROI\ position\ (yy) = i * ROI\ height \quad where\ i < Total\ number\ of\ row \tag{8.4}$$

$$Excess\ Green = 2 \times Green\ (G) - Red(R) - Blue(B) \tag{8.5}$$

After obtaining the plot image, the next work is to segment plants from the noisy background. Soil and shadows in the plot images were eliminated using excess green (E × G) thresholding (Eq. 8.5). The pixel with an E × G value less than the cutoff (25) was replaced with black (255, black). The cutoff value was chosen empirically and through visual observation of segmented images. Then the three middle rows of each plot were manually cropped for further investigation since they had been chemically treated differently by plant pathologists (Fig. 8.3).

Fig. 8.2 Dataset generation process **a** stitched image of corn filed for feeding to a plot splitting tool developed in ImageJ; **b** the plot spitting tool for generating plots from stitched image; **c** output of the plot splitting tool: samples plot images

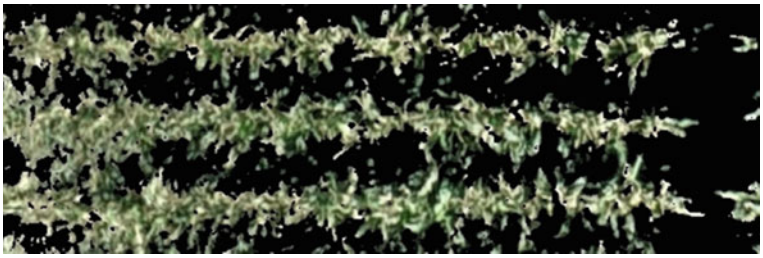

Fig. 8.3 Segmentation of plot images using excess green with threshold of 25

8.2.2 Preparation of Datasets

Three different datasets were prepared using the original plot images including non-augmentation, segmentation, augmentation. Non-augmentation dataset was prepared using 200 original plot images. Segmentation dataset also contained 200 plot images in which plants were segmented from backgrounds using E × G then cropping middle three rows of plants. Another dataset augmentation was prepared using original plot images in which geometric transformation techniques were used such as rotation, and flip (i.e., right, top, and random) (Table 8.1). The image rotation probability was set to 100%, implying that every image produced through augmentation was rotated slightly with a random chance. The parameters for rotation to the left were set to a maximum of 5 degrees and 10 degrees to the right (random rotation). With a probability of 50%, images were flipped to the left and right at random. Similarly, random flips from the top and bottom of the images were done with a 0.5 likelihood. Finally, images were zoomed randomly with a frequency of 30%, at a minimum scaling factor of 1.1, and a maximum scaling factor of 1.6. Augmentation dataset containing 6200 images, consisting of 3015 for high severity and 3185 for low severity. The parameters and techniques used for data augmentation is shown in Table 8.2. Photometric transformations were not used with the consideration that it might generate unreliable data with changed color values on individual pixels.

Table 8.1 Dataset description

Dataset	Description	Total	Training	Testing
Non augmentation	Original images	200	160	40
Segmentation	Original segmented images	200	160	40
Augmentation	Using augmentation techniques	6200	4960	1240

Table 8.2 Techniques used for preparing augmentation dataset

Augmentation techniques	Parameters	Values
Rotation	Probability, Angle	100%, 5°
Flipping (vertical, horizontal)	Probability	50%
Zooming	Probability, Scaling factors	30%, 1.1–1.6

8.2.2.1 Dataset for Training and Testing ML Algorithms

Features were extracted from all three datasets. A total of five textural features (i.e., contrast, dissimilarity, homogeneity, angular second moment, energy), nine color-based features (hue, saturation, value, red, green blue, lightness, and chromatic components *a and *b) were extracted. Gray-Level Co-occurrence Matrices (GLCMs) [6] based textural features were extracted. The code for textural were run in python (v3.8) using skimage python library. A function greycomatrix (image, distances, angles, levels, symmetric = False, normed = False) from the texture module was implemented. At first RGB images were converted into gray images using OpenCV. Images were fed to the function with 1-pixel distance offset, angle value of 90 and maximum 255 level to obtain GLCM matrices. Then the textural properties of the GLCM, such as contrast, dissimilarity, homogeneity, angular second moment was calculated using Eqs. (8.6), (8.7), (8.8), (8.9) and (8.10) respectively. Where i and j indicated the row and column number of the image window respectively; P_{ij} is the probability value in the cell i, j. Levels indicates number of rows or columns.

$$Contrast = \sum_{i,j=0}^{levels-1} P_{ij}(i-j)^2 \tag{8.6}$$

$$Dissimilarity = \sum_{i,j=0}^{levels-1} P_{ij} \mid i-j \mid \tag{8.7}$$

$$Homogeneity = \sum_{i,j=0}^{levels-1} \frac{P_{i,j}}{1+(i-j)^2} \tag{8.8}$$

$$Angular\,Second\,Moment(ASM) = \sum_{i,j=0}^{levels-1} P_{i,j}^2 \tag{8.9}$$

$$Energy = \sqrt{ASM} \tag{8.10}$$

Color features such red (R), green (G), and blue (B) pixel values were extracted from the datasets. Similarly, hue (H), saturation (S) value (V) features and lightness (L), chromatic components (*a and *b) were extracted images after converting RGB to HSV and L*a*b respectively. A total of 80% a dataset was used for training and remaining 20% were used for testing ML algorithms.

8.2.2.2 Dataset for Training and Testing DL Algorithms

The DL can extract features from the images automatically and it doesn't require handcrafted feature during training. Thus, features were not extracted from the datasets. All three datasets were used for modeling ML algorithms, but only augmentation dataset was used for modeling DL algorithms. The reason for excluding non-augmentation, and segmentation dataset for training DL was the insufficient number of training images. To avoid overfitting problem, only augmentation dataset were used for training DL algorithms.

8.2.3 Training and Validation of ML and DL Algorithms

ML algorithms were trained and validated on a computer configured with Intel® core™ i5-4300U CPU @ 1.90 GHz. Eight different machine learning classifiers were used to classify disease severity levels: Logistic Regression (LR), Ada Boost (AB), Gradient Boosting (GB), Support Vector Machine (SVM), Multilayer Perceptron (MLP), Random Forest (Rnaïveaive Bayes (NB), K-Nearest Neighbors (KNN). Machine learning algorithms were implemented using Scikit-learn [20] in python (v3.8). Parameters of ML algorithms were set default however the solver type and kernel for the LR and SVM was set to 'liblinear' and 'linear' respectively.

Two popular used DL algorithms (e.g., GoogLeNet and ResNet) were used for Goss's Wilt disease severity classifications. The DL algorithms were trained and validated on a computer configured with Intel® Core™ i7-4770 CPU @ 3.40 GHz. For consistency, both models' training epochs were set to 100. Cross entropy loss was used as the loss function, and stochastic gradient descent was used as the optimizer. The learning rate was set to 0.001, the momentum was set to 0.9, the step size was set to 7 and the gamma value was set to 0.1.

The performance of ML and DL algorithms were evaluated using precision, recall and F-score based on Eqs. 8.12, 8.13, and 8.14. True positive (TP) refers to correct predictions of high severity plots when plots are actually high severity. True negative (TN) indicates correct prediction of low severity plot when plots are actually low severity. False positive (FP) means incorrect predictions of high severity plots when plots are actually low severity. False negative (FN) indicates incorrect predictions of low severity plots when plots are actually high severity (Table 8.3).

Table 8.3 Confusion matrix for high severity and low severity class

		Predicted class	
		High severity	Low severity
Actual class	High severity	TP	FN
	Low severity	FP	TN

$$Precision = \frac{TP}{TP + FP} \tag{8.12}$$

$$Recall = \frac{TP}{TP + FN} \tag{8.13}$$

$$F - score = \frac{2 * Recall * Precision}{Recall + Precision} \tag{8.14}$$

8.2.4 Results

Regarding non-augmentation, GB achieved comparatively higher precision (0.85), recall (0.81) F-score (0.82) than other classifiers in this study (Table 8.4). In terms of precision (0.62) recall (0.61), and F-score (0.61), KNN had the lowest performance (Table 8.4). KNN achieved higher number of FN (10) than the other classifiers (Fig. 8.4). RF achieved comparatively similar precision (0.83), recall (0.78) and F-score (0.79) than the GB (Table 8.4).

On Segmentation dataset, RF achieved comparatively higher F-score (0.56) than other classifiers. LR and GB achieved similar precisions of 0.58 and 0.57, respectively and recalls of 0.56 and 0.57, respectively (Table 8.4). However, MLP achieved lowest precision (0.41) and F-score (0.40) comparatively to the other classifiers. MLP yielded highest FN (16) and lowest TP (3) than other classifiers (Fig. 8.4). Moreover, all the classifiers also yielded poor classification results (Table 8.4) (Fig. 8.5).

On augmentation dataset, RF classifiers outperformed other ML classifiers and achieved highest precision (0.99), recall (0.99) and F-score (0.99) (Table 8.4). It achieved higher TP (589) and TN (640) however, lower FN (5) and FP (6) among other classifiers (Fig. 8.6). The NB and MLP yielded lower precisions of 0.61 and 0.62 respectively, lower recall of 0.61 and 0.56 respectively and F-score of 0.60 and 0.51 respectively. The MLP and SVM yielded higher number of FN (465) higher number of FP (290) respectively (Fig. 8.6).

In this study, GoogLeNet and ResNet18 both performed good in classifying the disease severity. Though GoogleNet achieved 0.75 of precision, 0.70 of recall and 0.73 of F-score, Resnet18 yielded comparatively better precision (0.81), recall (0.78) and F-score (0.79). GoogleNet and ResNet both performed lower than ML classifier (RF) in terms of precision, recall and F-score on augmentation dataset (Table 8.5).

Figures 8.7 and 8.8 showed accuracy and loss curve of GoogLeNet and ResNet18 respectively. The lower gaps between training and validation loss indicated that the ResNet18 is good fitted with the dataset and free from overfitting problems (Fig. 8.8).

Table 8.4 Performance comparison of different machine learning (ML) algorithms in classifying Goss's Wilt disease severity on different types of dataset

Datasets	Machine learning classifiers	Precision	Recall	F-score
No augmentation	Logistic regression	0.79	0.76	0.76
	Ada boost	0.72	0.72	0.72
	Gradient boosting	0.85	0.81	0.82
	Support vector machine	0.80	0.73	0.73
	Multilayer perceptron	0.74	0.71	0.71
	Random forest	0.83	0.78	0.79
	Naive Bayes	0.82	0.76	0.76
	K-nearest neighbors	0.62	0.61	0.61
Segmentation	Logistic regression	0.58	0.56	0.54
	Ada boost	0.55	0.54	0.53
	Gradient boosting	0.57	0.57	0.57
	Support vector machine	0.55	0.54	0.52
	Multilayer perceptron	0.41	0.44	0.40
	Random forest	0.57	0.57	0.56
	Naive Bayes	0.43	0.42	0.42
	K-nearest neighbors	0.46	0.47	0.45
Augmentation	Logistic regression	0.68	0.67	0.67
	Ada boost	0.80	0.80	0.79
	Gradient boosting	0.89	0.89	0.89
	Support vector machine	0.73	0.71	0.70
	Multilayer perceptron	0.62	0.56	0.51
	Random forest	0.99	0.99	0.99
	Naive Bayes	0.61	0.61	0.60
	K-nearest neighbors	0.94	0.94	0.94

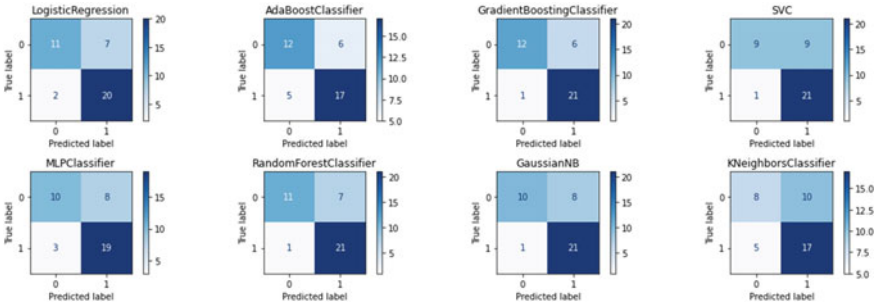

Fig. 8.4 Confusion matrix of classifications on non-augmentation dataset

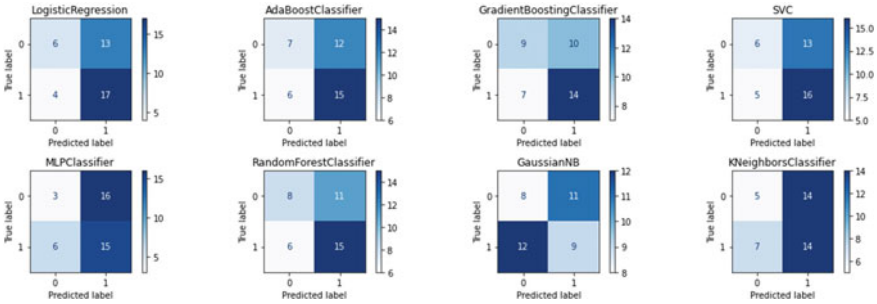

Fig. 8.5 Confusion matrix of classifications on segmentation dataset

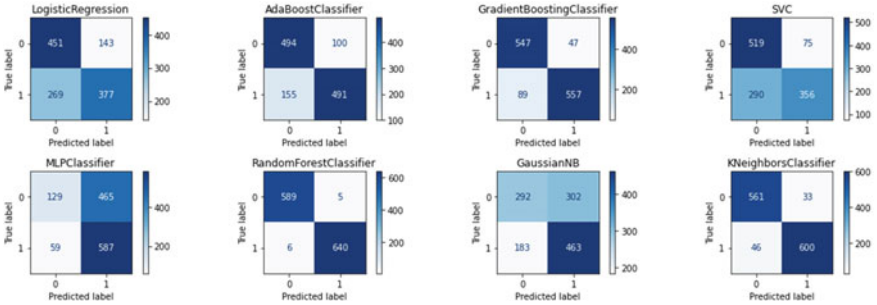

Fig. 8.6 Confusion matrix of classifications on augmentation dataset

Table 8.5 Evaluation matrices of Deep learning algorithms obtained during validation

Deep Learning Classifiers	Precision	Recall	F-score
GoogleNet	0.75	0.70	0.73
ResNet18	0.81	0.78	0.79

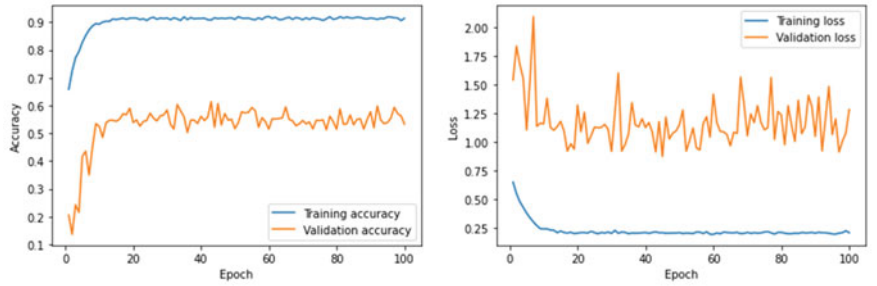

(a) **(b)**

Fig. 8.7 Accuracy and loss curve of GoogLeNet. **a** Training accuracy of 90% with 1–1.5% of training loss; **b** validation accuracy of 50 to 60% and 2.5% validation loss

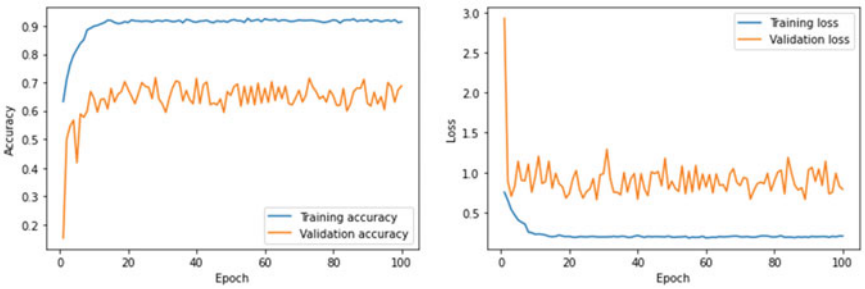

Fig. 8.8 Accuracy and loss curve of ResNet18. **a** ResNet18 yielded around 90% of training accuracy and validation accuracy around 60–70%. **b** Training loss decreased gradually and reached 0% and validation loss reached between 0.5 and 1.5%

8.2.5 Discussion

The ML based algorithms constantly performed poor in terms of Precision, Recall and F-score on segmentation dataset. The probable reason for underperforming ML models on segmentation dataset was loss of information during segmentation. Plots were segmented using the threshold a value (25) which were determined empirically or manually. Dataset contained plot images from five different heights. The images from higher height might lose information higher than shorter heights which requires further investigations. RF algorithm outperformed other ML and DL based algorithms in this study and achieved F-score of 0.99. Conversely DL algorithms can extract features automatically and avoid manual feature extraction and selection process. Data augmentation enhanced the number of instances in training dataset helps ML and DL algorithms learn from adequate dataset.

8.2.6 Conclusion

This study concluded that ML algorithm (Random Forest) performed better in Goss's Wilt disease severity assessment in augmentation dataset, which can be recommended for severity assessment in future practical application. Random Forest yielded higher precision (0.99), recall (0.99) and F-score (0.99) among all ML algorithms. Random Forest can be incorporated to unmanned aerial imagery to build an automatic Goss's Wilt disease assessment system. ML models performed poor on the segmentation dataset. The effect of flight height on classification accuracy has not been investigated due to data limitations of individual heights (Total 40 images; training set: 32 images; testing set: 8 images). This could lead to model overfitting in ML. The effect of heights on accuracies will be investigated in future.

Acknowledgements Authors would like to express their gratitude to Jensen Kenton for his preliminary processing images collected by the unmanned aerial vehicle, which includes stitching them using Pixle4D and georeferencing them using ArcGIS10. Additionally, the authors would like to thank Dr. Friskop's specialists for assisting in the preparation of the experimental sites. This study was conducted in collaboration with the North Dakota Corn Commission and the USDA Agricultural Research Service under the project No. 6064-21660-001-32S. Project accession No. 435589.

References

1. Abdulridha J, Batuman O, Ampatzidis Y (2019) UAV-based remote sensing technique to detect citrus canker disease utilizing hyperspectral imaging and machine learning. Remote Sens 11(11):1373
2. Chemura A, Mutanga O, Sibanda M, Chidoko P (2018) Machine learning prediction of coffee rust severity on leaves using spectroradiometer data. Tropical Plant Pathology 43(2):117–127
3. Das AK, Friskop A, Flores P, Igathinathan C, Mathew JJ, Zhang Z (2021) Using aerial imagery coupled with machine learning to assess Goss's Wilt disease severity in field corn. In: 2021 ASABE annual international virtual meeting. American Society of Agricultural and Biological Engineers
4. Flores P, Zhang Z (2021) Wheat lodging ratio detection based on UAS imagery coupled with different machine learning and deep learning algorithms. Smart Agric 3(2):23–34
5. Greg Endres (2018, December 3) Goss's leaf blight and wilt of corn—carrington REC. https://www.ag.ndsu.edu/carringtonrec/center-points/2018/goss2019s-leaf-blight-and-wilt-of-corn
6. Haralick RM, Shanmugam K, Dinstein IH (1973) Textural features for image classification. IEEE Trans Syst Man Cybern 6:610–621
7. Jahan N, Flores P, Liu Z, Friskop A, Mathew J, Zhang Z (2020) Detecting and distinguishing wheat diseases using image processing and machine learning algorithms. ASABE Paper No. 2000372. St. Joseph, MI: ASABE. https://doi.org/10.13031/aim.202000372
8. Jahan N, Zhang Z, Liu Z, Friskop A, Flores P, Mathew J, Das A (2021) Using images from a handheld camera to detect wheat bacterial leaf streak disease severities. ASABE Paper No. 2100112. St. Joseph, MI: ASABE. https://doi.org/10.13031/aim.202100112
9. Kerkech M, Hafiane A, Canals R (2018) Deep leaning approach with colorimetric spaces and vegetation indices for vine diseases detection in UAV images. Comput Electron Agric 155:237–243
10. Kerkech M, Hafiane A, Canals R (2020) Vine disease detection in UAV multispectral images using optimized image registration and deep learning segmentation approach. Comput Electron Agric 174:105446
11. Kusumo BS, Heryana A, Mahendra O, Pardede HF (2018) Machine learning-based for automatic detection of corn-plant diseases using image processing. In: 2018 international conference on computer, control, informatics and its applications (IC3INA). IEEE, pp 93–97
12. Lee K, An H, Park C, So K, Na S, Jang S (2019) Estimation of rice grain yield distribution using UAV imagery. J Korean Soc Agric Eng 61(4):1–10
13. Liang Q, Xiang S, Hu Y, Coppola G, Zhang D, Sun W (2019) PD2SE-Net: Computer-assisted plant disease diagnosis and severity estimation network. Comput Electron Agric 157:518–529
14. Liu Z, Du Z, Peng Y, Tong M, Liu X, Chen W (2020, June) Study on corn disease identification based on PCA and SVM. In: 2020 IEEE 4th information technology, networking, electronic and automation control conference (ITNEC), vol 1. IEEE, pp 661–664
15. Mathew J, Zhang Y, Flores P, Igathinathane C, Zhang Z (2021) Development and testing of an RGB-D camera-based rock detection system and path optimization algorithm in an indoor environment. ASABE Paper No. 2100105. St. Joseph, MI: ASABE. https://doi.org/10.13031/aim.202100105

16. Meng R, Lv Z, Yan J, Chen G, Zhao F, Zeng L, Xu B (2020) Development of spectral disease indices for southern corn rust detection and severity classification. Remote Sens 12(19):3233
17. Mogili UR, Deepak BBVL (2018) Review on application of drone systems in precision agriculture. Procedia Comput Sci 133:502–509
18. Panigrahi KP, Das H, Sahoo AK, Moharana SC (2020) Maize leaf disease detection and classification using machine learning algorithms. In: Progress in computing, analytics and networking. Springer, Singapore, pp 659–669
19. Parikh A, Raval MS, Parmar C, Chaudhary S (2016, October) Disease detection and severity estimation in cotton plant from unconstrained images. In: 2016 IEEE international conference on data science and advanced analytics (DSAA). IEEE, pp 594–601
20. Pedregosa F, Varoquaux G, Gramfort A, Michel V, Thirion B, Grisel O, …, Duchesnay E (2011) Scikit-learn: machine learning in Python.J Mach Learn Res 12:2825–2830
21. Raeva PL, Šedina J, Dlesk A (2019) Monitoring of crop fields using multispectral and thermal imagery from UAV. Eur J Remote Sens 52(sup1):192–201
22. Ren T, Zhang Y, Wang C (2019, September) Identification of corn leaf disease based on image processing. In: 2019 2nd international conference on information systems and computer aided education (ICISCAE). IEEE, pp 165–168
23. Salgadoe ASA, Robson AJ, Lamb DW, Dann EK, Searle C (2018) Quantifying the severity of phytophthora root rot disease in avocado trees using image analysis. Remote Sens 10(2):226
24. Santoso H, Tani H, Wang X, Prasetyo AE, Sonobe R (2019) Classifying the severity of basal stem rot disease in oil palm plantations using WorldView-3 imagery and machine learning algorithms. Int J Remote Sens 40(19):7624–7646
25. Singh V, Misra AK (2017) Detection of plant leaf diseases using image segmentation and soft computing techniques. Inf Process Agric 4(1):41–49. https://doi.org/10.1016/j.inpa.2016.10.005
26. Stroppiana D, Villa P, Sona G, Ronchetti G, Candiani G, Pepe M, ... , Boschetti M (2018) Early season weed mapping in rice crops using multi-spectral UAV data. Int J Remote Sens 39(15–16):5432–5452
27. USDA ERS—Feedgrains Sector at a Glance. (n.d.). Retrieved May 3, 2021, from https://www.ers.usda.gov/topics/crops/corn-and-other-feedgrains/feedgrains-sector-at-a-glance
28. Wang G, Sun Y, Wang J (2017) Automatic image-based plant disease severity estimation using deep learning. Comput Intell Neurosci. https://doi.org/10.1155/2017/2917536
29. Yao L, Hu D, Zhao C, Yang Z, Zhang Z (2021) Wireless positioning and path tracking for a mobile platform in greenhouse. Int J Agric Biol Eng 14(1):216–223. https://doi.org/10.25165/j.ijabe.20211401.5627
30. Zhang J, Wan L, Igathinathane C, Zhang Z, Guo Y, Sun D, Cen H (2021b) Spatiotemporal heterogeneity of chlorophyll content and fluorescence response within rice (Oryza sativa L.) Canopies under different nitrogen treatments. Front Plant Sci 12, 499. https://doi.org/10.3389/fpls.2021.645977
31. Zhang Z, Flores P (2021) Detection of wheat lodging plots using indices derived from multispectral and visible images. In: Li J, Zhang Z (eds) Nondestructive evaluation of agro-products by intelligent sensing techniques. Sharjah, United Arab Emirates, pp 1–299. https://doi.org/10.2174/9789811485800121010 1
32. Zhang Z, Flores P, Igathinathane C, Naik LD, Kiran R, Ransom JK (2020) Wheat lodging detection from UAS imagery using machine learning algorithms. Remote Sens 12(11):1838. https://doi.org/10.3390/rs12111838
33. Zhang Z, Heinemann PH, Liu J, Baugher TA, Schupp JR (2016) The development of mechanical apple harvesting technology: a review. Trans ASABE 59(5):1165–1180. https://doi.org/10.13031/trans.59.11737
34. Zhang Z, Igathinathane C, Li J, Cen H, Lu Y, Flores P (2020) Technology progress in mechanical harvest of fresh market apples.Comput Electron Agric 175:105606. https://doi.org/10.1016/j.compag.2020.105606
35. Zhang Z, Lu Y, Lu R (2021) Development and evaluation of an apple infield grading and sorting system. Postharvest Biol Technol 180:111588. https://doi.org/10.1016/j.postharvbio.2021.111588